ANATOMY OF HH 111 FROM CO OBSERVATIONS: A BOW-SHOCK-DRIVEN MOLECULAR OUTFLOW

BERTRAND LEFLOCH,[1] JOSÉ CERNICHARO,[2] BO REIPURTH,[3] JUAN RAMON PARDO,[2] AND ROBERTO NERI[4]

ABSTRACT

We present single-dish and interferometric millimeter line observations of the HH 111 outflow and its driving source. The physical conditions of the core have been determined from the emission of the millimeter line of CO and its isotopomers and CS with the IRAM 30 m telescope, and the CO $J = 7 \rightarrow 6$ line with the Caltech Submillimeter Observatory. The emission reveals a small condensation of cold ($T = 20$–25 K) and dense gas [$n(H_2) = 3 \times 10^5$ cm^{-3}]. The outflow has been mapped with the IRAM Plateau de Bure interferometer (PdBI). The cold gas is distributed in a hollow cylinder surrounding the optical jet. The formation of this cavity and its kinematics are well accounted for in the frame of outflow gas entrainment by jet bow shocks. Evidence of gas acceleration is found along the cavity walls, correlated with the presence of optical bow shocks. The separation of the inner walls reaches $8''$–$10''$, which matches the transverse size of the wings in the bow shock. CSO observations of the $J = 7 \rightarrow 6$ line show evidence of a high-velocity and hot gas component ($T = 300$–1000 K) with a low filling factor. This emission probably arises from shocked gas in the jet. Observations of the $^3P_2$–$^3P_1$ [C I] line are consistent with C-type nondissociative shocks. Mapping of the high-velocity molecular bullets B1–B3, located beyond the optical jet, reveals small structures of $3'' \times 7''$ flattened perpendicular to the flow direction. They are made of cold ($T \sim 30$ K), moderate density gas [$n(H_2) = (0.5$–$1.0) \times 10^4$ cm^{-3}], expanding into the low-density surrounding medium. Their properties are consistent with their being shocked gas knots resulting from past time-variable ejections in the jet.

Subject headings: ISM: clouds — ISM: individual (HH 111) — ISM: jets and outflows — stars: formation

1. INTRODUCTION

Herbig-Haro jets are manifestations of the accretion processes that are involved in the birth of stars, and as such represent a fossil record of the recent activity of their driving sources. The study of jets thus enables us to understand the past history of young stars as they build up their mass. As these jets penetrate their ambient medium, they transfer momentum and accelerate their surroundings, and it appears that it is this interaction that causes the ubiquitous molecular outflows. For a recent review on these issues, see Reipurth & Bally (2001).

One of the finest HH jets known is the HH 111 jet, located in the L1617 cloud in Orion (Reipurth 1989). It has a very highly collimated body, with a large number of individual knots, and has large proper motions (300–600 km s^{-1}). The jet flows at an angle of only $10°$ to the plane of the sky (Reipurth et al. 1992). Beyond the collimated jet the flow continues, and it is in fact only a minor part of a truly gigantic bipolar HH complex stretching over 7.7 pc (Reipurth et al. 1997a). Optical spectra are discussed by Morse et al. (1993a, 1993b) and Noriega-Crespo et al. (1993). Near-infrared observations have revealed a remarkable symmetry between the optical jet and a near-infrared counterjet and that a second bipolar flow, HH 121, emerges from the source, suggesting that it is a binary (Gredel & Reipurth 1993, 1994; Davis et al. 1994; Coppin et al. 1998; Reipurth et al. 2000). The optical jet is coaxial with a major well-collimated molecular outflow (Reipurth & Olberg 1991; Cernicharo & Reipurth 1996; Nagar et al. 1997; Lee et al. 2000). Beyond the visible

jet, Cernicharo & Reipurth (1996, hereafter CR96) found a set of three high-velocity CO bullets, which apparently represent working surfaces that no longer produce optical shock emission. The jet is driven by IRAS 05491+0247, a Class I source with a luminosity of about 25 $L_\odot$, surrounded by cold dust and gas (Reipurth et al. 1993; Stapelfeldt & Scoville 1993; Yang et al. 1997; Dent et al. 1998). A small 3.6 cm radio continuum jet was detected around the source by Rodríguez & Reipurth (1994). Recently, infrared images obtained with the *Hubble Space Telescope* (*HST*) have revealed that another source is located only $3''$ from the main one, which itself is a binary judging from the quadrupolar outflows; so altogether, it appears that the driving source is part of a hierarchical triple system (Reipurth et al. 1999). In fact, the entire giant jet flow may be a result of the dynamical interactions between the three members of this triple system (Reipurth 2000).

The short blue lobe found by Reipurth & Olberg (1991) appears to be a highly collimated molecular jet about $90''$ long with a collimation factor of 9 (see their Figs. 2–4) in the $12''$ data of CR96. The blue lobe ends at the bow shock P and the optical knots Q, R, and S. Nagar et al. (1997) showed an interferometric map at $6''$ resolution of the $J = 1 \rightarrow 0$ line, which allowed them to resolve the structure of the low-velocity gas around the optical jet. The main features of the ionized and molecular gas in HH 111 are summarized in Figure 1.

In this paper we present single-dish and high-resolution interferometric observations of the body of HH 111, the protostellar core and the high-velocity CO bullets. We characterize the gas kinematics and the physical conditions in the gas and report the detection of a hot temperature component in the outflow. We discuss these results in relation to current theories on the coupling of HH jets and molecular outflows.

We find that the molecular gas entrainment in the outflow is well accounted for in the frame of jet bow-shock-driven outflows, as modeled by Raga & Cabrit (1993; hereafter RC93).

[1] Laboratoire d'Astrophysique de l'Observatoire de Grenoble, Grenoble, France.
[2] Instituto de Estructura de la Materia, Departamento Física Molecular, Madrid, Spain.
[3] Institute for Astronomy, University of Hawaii, Hilo, HI.
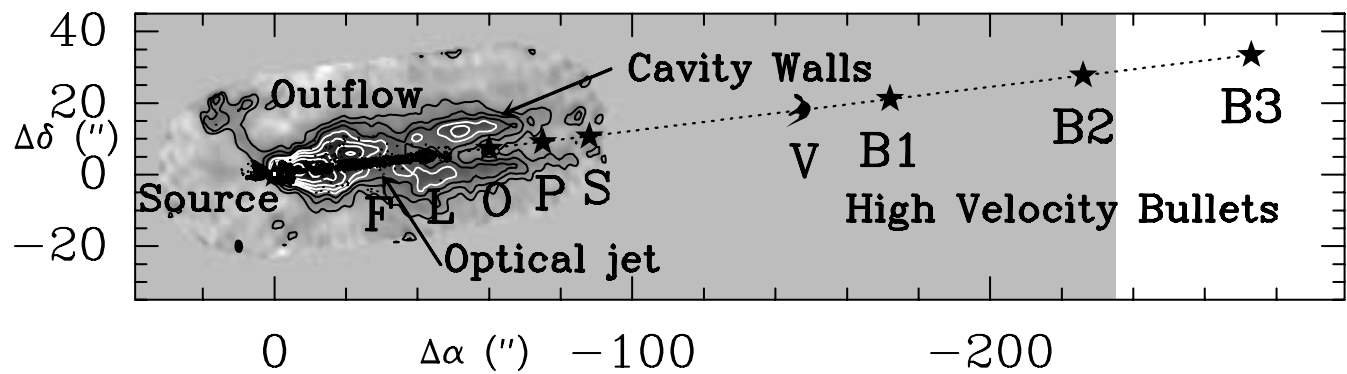[4] Institut de Radioastronomie Millimétrique, Domaine Universitaire, St. Martin d'Hères, France.

Fig. 1.—Map of the CO $J = 1 \rightarrow 0$ outflow emission integrated between +0.25 km s^{-1} and +7.3 km s^{-1} obtained with the IRAM Plateau de Bure interferometer. We have indicated the main features detected in the molecular gas (the cavity and the high-velocity bullets) and in the ionized gas (the optical jet, as observed with *HST*, the shocked knots, and the large bow shock V). A dotted line traces the main axis of the jet.

Preliminary results were reported by Reipurth & Cernicharo (1995) and Cernicharo et al. (1997).

2. OBSERVATIONS

2.1. *Single-Dish Data*

The central source and the HH 111 outflow were observed in the millimeter lines of CS and the CO isotopomers with the IRAM 30 m telescope in 1990 and 1994. The CO observations have already been presented in CR96. For these observations, we used as spectrometer an autocorrelator with 2048 channels and spectral resolution of 37 kHz. The spectral resolution was degraded to ≈ 0.2 km s^{-1}. The results are expressed in units of main-beam brightness temperature. The main-beam efficiency was measured to be 0.63 and 0.57 at the frequency of the CS $J = 2 \rightarrow 1$ and $J = 3 \rightarrow 2$ transitions, respectively.

The CO $J = 7 \rightarrow 6$ line at 806.651708 GHz was observed toward the central source and bullet B3 with the Caltech Submillimeter Observatory (CSO) in 2005 December. The receiver was tuned in double-sideband and the system temperature ranged between 5700 and 7500 K. This allowed us to observe simultaneously the $^3P_2-^3P_1$ [C I] lines at 809341.97 GHz in the image band. An acousto-optical spectrometer (AOS) was used as spectrometer, which provided a kinematical resolution of 0.24 km s^{-1}. At this frequency, the beam size of the telescope is about 12″ and the beam efficiency is 0.28. The calibration was checked toward Ori IRc2 in Orion A.

2.2. *Interferometric Data*

The CO $J = 1 \rightarrow 0$ emission along the HH 111 outflow was observed with the IRAM Plateau de Bure interferometer (PdBI; see Table 1). A mosaic of five fields was performed; the field centers were located at the offset positions $(+10″, 0)$, $(-10″, +3″)$,

$(-30″, +6″)$, $(-50″, +9″)$, and $(-70″, +12″)$ with respect to the source, $05^h51^m46.2^s$, $+02°48′29.5″$ (J2000.0). QSO 0528+134 and 3C 120 were used as phase calibrators. An autocorrelator was used as spectrometer, with an element of resolution of 20 kHz, corresponding to a kinematic resolution of ≈ 0.06 km s^{-1} at the CO $J = 1 \rightarrow 0$ frequency. The IRAM 30 m data of the region obtained by CR96 were used to provide the short spacings and combined with the PdBI visibilities. The combined map is shown in Figure 5. The synthetic beam is $3.79″ \times 2.43″$ at 2.6 mm and makes a P.A. of $-4°$ with respect to north.

The CO $J = 2 \rightarrow 1$ emission of the high-velocity bullets B1, B2 and B3 discovered outside the molecular cloud was observed with the IRAM PdBI in 1996. Three fields were observed, centered at $05^h51^m34.65^s, +02°48′50.50″$ (B1), $05^h51^m31.12^s, +02°48′57.50″$ (B2), and $05^h51^m28.06^s, +02°49′08.02″$ (B3). The same phase calibrators as before were used. The resolution of the autocorrelator was set to 160 kHz, which provided a kinematic resolution of ≈ 0.16 km s^{-1} at the CO $J = 2 \rightarrow 1$ frequency. The synthetic beam is $1.96″ \times 1.26″$ at 1.3 mm and makes a P.A. of $-192°$ with respect to north.

To estimate the fraction of flux missed by the interferometer, we have compared the flux measured at the IRAM 30 m telescope with the flux recovered by the interferometer toward bullet B2 in the velocity interval of maximum intensity intensity. At the IRAM 30 m the line intensity peak is 0.43 K, which corresponds to a total flux of 5.1 Jy, after correcting for the source convolution with the beam and taking into account the antenna efficiency of 10 Jy K^{-1} at 1.3 mm. At the same velocity (-36.8 km s^{-1}), the flux integrated over the reconstructed source was estimated with the FLUX procedure and found to be 4.95 Jy. We conclude that almost all the flux has been recovered by the interferometer.

3. THE SOURCE

Figure 2 shows the emission of the millimeter lines of CS and the CO isotopomers detected toward the VLA source and two nearby positions offset by 20″ in right ascension. In the direction of the VLA source, double-peaked profiles are detected in all lines of various opacities, but the C^{18}O $J = 1 \rightarrow 0$ and ^{13}CO $J = 1 \rightarrow 0$ (see, e.g., CS $J = 2 \rightarrow 1$ and ^{13}CO $J = 2 \rightarrow 1$). In particular, the maximum of the singly peaked ^{13}CO $J = 1 \rightarrow 0$ coincides with the 8.4 km s^{-1} peak of the $J = 2 \rightarrow 1$ transition. This allows us to exclude self-absorption as origin of the double peaked profiles detected.

The ^{13}CO interferometric map of HH 111 by Stapelfeldt & Scoville (1993) indicates a north-south velocity gradient in the direction of the core where the powering source of HH 111 has

TABLE 1
PHYSICAL PARAMETERS OF THE CO BULLETS MAPPED WITH THE PdBI

| | POSITION (J2000.0) | | SIZE | MASS | DENSITY |
BULLET	R.A.	Decl.	(arcsec)	($10^{-4} M_\odot$)	(10^4 cm^{-3})
B1..........	05 51 34.9	02 48 51.1	3.3×4.6	3.1	1.5
B2..........	05 51 31.4	02 48 57.7	3.3×6.7	2.1	0.59
B3..........	05 51 29.0	02 49 08.0	3.3×6.7	1.9	0.53

NOTE.—Units of right ascension are hours, minutes, and seconds, and units of declination are degrees, arcminutes, and arcseconds.
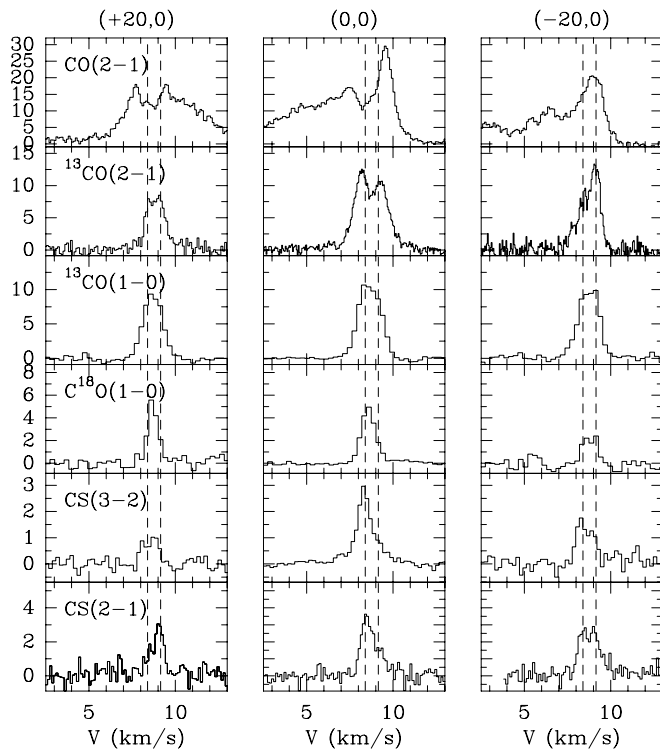
FIG. 2.—Molecular emission of CO, ^{13}CO, C^{18}O, and CS toward selected positions along the optical jet of HH 111, indicated above each column. The dashed lines mark the velocity of the protostellar core ($v = 8.4$ km s^{-1}) and the cavity wall ($v = 9.2$ km s^{-1}).
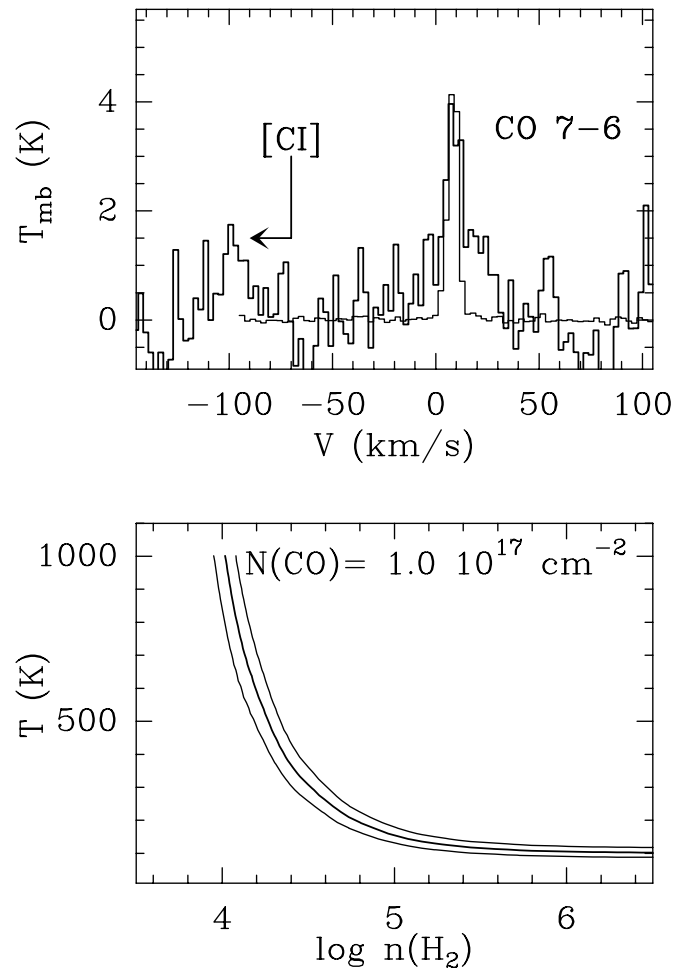

FIG. 3.—*Top*: CO $J = 7 \rightarrow 6$ observed toward the central source (*thick line*). We have superposed the $J = 2 \rightarrow 1$ line emission (*thin line*) detected with the IRAM 30 m telescope. *Bottom*: Variations of the 7–6/2–1 ratio R as a function of the kinetic temperature and density. Calculations were done for a CO column density of 1.0×10^{17} cm^{-2} in the LVG approximation. The contours at 0.8, 1.0, and 1.2 times the measured ratio $R = 3.0$ are drawn.

been formed. The CS map of Yang et al. (1997) taken with the Nobeyama interferometer also suggests such a velocity gradient. It has been interpreted by Yang et al. (1997) as due to infalling gas around the exciting source of HH 111. However, the fact that the emission from the CS lines show wings associated with the molecular outflow renders difficult the interpretation of the data. Indeed, the gas kinematics is affected by several different physical processes, as evidenced by the presence of a well-defined cavity (see § 4.3; also CR96 and Nagar et al. 1997).

We do not detect any spatial shift in the velocity centroid of the molecular emission in the direction perpendicular to the outflow. Hence, the double-peaked line profiles are not tracing the collapsing gas of the protostellar envelope, but most likely the interaction of the jet with the ambient gas, constituting the rear part of an expanding cavity around the optical jet. This point is addressed more thoroughly in § 4.

The C^{18}O $J = 1 \rightarrow 0$ transition traces the emission of the parental core at 8.4 km s^{-1}. The C^{18}O and ^{13}CO $J = 1 \rightarrow 0$ were observed simultaneously by the same receiver (they lie in the same intermediate-frequency [IF] band), which offers the advantage of eliminating the uncertainties in the pointing and the relative calibration. Toward the source, we measure main-beam brightness temperatures $T^{18} = 4.9$ K and $T^{13} = 10.6$ K for the C^{18}O and the ^{13}CO transitions, respectively. Both transitions are thermalized at the density of the core. Assuming a standard relative abundance ratio $[^{13}$CO]/[C^{18}O] = 8, we derive an opacity $\tau_{10}^{18} = 0.56$ for the C^{18}O line. Analysis of the C^{18}O transition in the large-velocity gradient (LVG) approximation yields a gas column density $N($C^{18}O$) = 6.5 \times 10^{15}$ cm^{-2} and a temperature of 15 K. Hence, the total gas column density of the core is $N($H$_2) = 3.3 \times 10^{22}$ cm^{-2}.

The CO $J = 7 \rightarrow 6$ to $J = 2 \rightarrow 1$ intensity line ratio measured at ambient velocities, between +3.8 and +11.5 km s^{-1} (see

§ 4.1), is $\approx$0.3, as expected for gas at 20–25 K and densities of 10^4–10^5 cm^{-3}. We therefore adopt a value of 20 K in what follows.

The dense gas tracers (CS) peak at $v_{\rm lsr} = 8.4$ km s^{-1} in the central core region. The lines are rather bright ($T_{\rm mb} = 3$ K) and narrow (Δv less than 1 km s^{-1}). Small wings are detected between 6.5 and 11 km s^{-1} (Fig. 2). The emission draws a round condensation of 26$''$ diameter (beam deconvolved) or 0.06 pc. Analysis of the CS $J = 3 \rightarrow 2$ and $J = 2 \rightarrow 1$ transitions in the LVG approximation yields typical densities of $n($H$_2) = 3 \times 10^5$ cm^{-3} and column densities $N($CS$) = 1.3 \times 10^{13}$ cm^{-2} at the brightness peak. The lines are optically thin, with $\tau^{21} = 0.44$ and $\tau^{32} = 0.77$.

Emission in the $^3P_2$–$^3P_1$ [C I] line was detected at the velocity of the ambient gas $\simeq$9 km s^{-1} (Fig. 3; note that the [C I] line is in the image band). A Gaussian fit to this emission yields an integrated flux of 20 K km s^{-1}, peak intensity of 1.5 K, and a line width of 12 km s^{-1}. Such a broad line width implies that the [C I] emission arises from the outflow and not only from the ambient gas. This suggests a gas column density of 1.0×10^{18} cm^{-2} for a temperature of 20 K. The ratio of atomic carbon to carbon monoxide column densities is therefore [C I]/CO $\simeq$ 0.3, a typical value measured in the Orion molecular cloud.

4. THE OUTFLOW

4.1. *Hot Gas near the Source*

No evidence of high-velocity wings was found toward the central source in the low $J = 1 \rightarrow 0$ and $J = 2 \rightarrow 1$ CO line profiles obtained with the IRAM telescope (CR96; see also Fig. 3). CR96 pointed out that in case the outflowing gas would have a high excitation temperature, much above the 15–20 K estimated from the lowest two transitions, the opacity of the latter would be very low, making them extremely difficult to detect.

Hatchell et al. (1999) showed evidence for warm gas in the range 80–150 K in the HH 111 high-velocity bullets from observations in the CO $J = 4 \rightarrow 3$ and $J = 3 \rightarrow 2$ transitions. We have observed the central source in the high $J = 7 \rightarrow 6$ CO transition at the CSO; the upper energy level lies at 155 K above the ground state and is a much more sensitive probe of warm gas.

The final spectrum is displayed in Figure 3. The kinematical resolution was degraded to 2.4 km s^{-1} to improve the signal-to-noise ratio. The rms is 0.20 K per velocity channel. We have superposed the $J = 2 \rightarrow 1$ spectrum obtained with the IRAM 30 m telescope, scaled to match the brightness peak of the $J = 7 \rightarrow 6$ line. The half-power beam width (HPBW) of both telescopes are similar at the concerned frequencies. We detect high-velocity wings at both blue- and redshifted velocities, with a signal-to-noise ratio of 4 σ and above 5 σ, respectively. Emission is detected at velocities larger than 30 km s^{-1} with respect to the source. These wings are barely seen in the $J = 2 \rightarrow 1$ line. The $J = 7 \rightarrow 6$ line emission can therefore be divided in three velocity intervals: the blueshifted wing (-40 to $+3.8$ km s^{-1}), the "ambient" gas ($+3.8$ to $+13$ km s^{-1}), and the redshifted wing ($+13$ to $+40$ km s^{-1}).

As illustrated in Figure 3, the relative intensity of the CO $J = 7 \rightarrow 6$ with respect to the $J = 2 \rightarrow 1$ is much larger in the wings than in the ambient gas, which indicates highly different physical conditions, in particular, a much higher temperature. We have estimated the physical conditions in the high-velocity wings from modeling both lines in the LVG approach. We have adopted the CO collisional coefficients determined by Flower (2001) for CO-ortho-H$_2$ collisions in the range $5-400$ K. For temperatures beyond 400 K, the collisional coefficients are extrapolated adopting a temperature dependence of $(T/400 \text{ K})^{1/2}$. The signal-to-noise ratio in the wings is not high enough to study the excitation conditions as a function of velocity. Therefore, we consider the emission integrated over the velocity interval assigned to each wing. We obtain a similar $J = 7 \rightarrow 6/J = 2 \rightarrow 1$ line ratio of ≈ 3. This value is probably a lower limit as the filling factor of the $J = 7 \rightarrow 6$ is probably less than that of the $J = 2 \rightarrow 1$. The LVG calculations show that in order to account for a $J = 7 \rightarrow 6/J = 2 \rightarrow 1$ line ratio of ≈ 3, the kinetic temperature must be above 100 K *at least*, and the density must be larger than a few $\times 10^3$ cm^{-3} (see Fig. 3). In this range of density and column density, the $J = 2 \rightarrow 1$ transition is thermalized, but the $J = 7 \rightarrow 6$ transition is not; the $J = 2 \rightarrow 1$ transition is optically thin, while the $J = 7 \rightarrow 6$ transition is optically thick.

The velocity of this hot gas is very large, up to 150 km s^{-1} when deprojected. If the emission arises from entrained gas, then the density of the hot gas is probably much less than in the cold low-velocity gas, where we estimate $n(\text{H}_2) = 7 \times 10^4$ cm^{-3} (see § 4.2). The density of the hot CO gas is at most a few times 10^4 cm^{-3}, which implies a temperature of about 300–1000 K or more. Spectroscopic diagnostics in the optical range indicate typical densities of 7000 cm^{-3} in the jet (Hartigan et al. 1994).

The CO column density of entrained gas in each wing lies in the range $(0.3-1.0) \times 10^{17}$ cm^{-2}. The mass of warm H$_2$ is about $(0.3-1.0) \times 10^{-2}$ $M_\odot$ per beam, and the associated momentum is 0.3–1.0 $M_\odot$ km s^{-1}, assuming a filling factor of 1. Integrated over the cavity, the mass of warm gas would amount to 0.02–0.07 $M_\odot$, and the velocity-deprojected momentum would be $\simeq 2-7$ $M_\odot$ km s^{-1}. The overall momentum carried away in the hot CO gas would be a factor of 10 larger than in the low-velocity cold gas and the high-velocity molecular jet (Nagar et al. 1997; CR96). We conclude that the filling factor of the hot component is probably much smaller than 1. For a filling factor of 0.1, the same amount of momentum is carried away by the three components (molecular jet, high-velocity wings, and low-velocity "cavity"). As a consequence, the hot CO emission is to arise from a narrow region in/around the optical jet, and the size of the emitting region is a few arcseconds. However, we cannot exclude the possibility that the emission arises from the whole cavity. If so, Kelvin-Helmholtz instabilities should grow along the jet. This has not been observed by *HST*. As discussed by Reipurth et al. (1997b; hereafter RHH97) the optical jet propagates into a very low density medium ($n \sim 350$ cm^{-3}). Therefore, we favor the hypothesis that the hot CO gas emission comes from the jet itself.

The spectra obtained by CR96 in the CO $J = 2 \rightarrow 1$ line further west in the flow, toward optical knots P–S, show similar line wing profiles, typically 30 km s^{-1} wide, with maximum intensity at the ambient gas velocity, *plus* the signature of the molecular jet detected as a 5–8 km s^{-1} wide isolated velocity component centered at ≈ -60 km s^{-1} (see Figs. 3a and 3b). Assuming similar excitation conditions in the jet, i.e., a $J = 7 \rightarrow 6/J = 2 \rightarrow 1$ line intensity ratio of 3, we would expect a $J = 7 \rightarrow 6$ line intensity of $\simeq 0.4$ K, which is below the detection limit allowed by our data.

When averaging the $J = 2 \rightarrow 1$ line profiles over the low-velocity outflow emission region, between the source and offset $-70''$, a weak high-velocity component is detected at the 4 σ level, which peaks at the same velocity as in the jet (see Fig. 4c). Its narrow line width ($\Delta v \simeq 3$ km s^{-1}) is consistent with a motion parallel to the optical jet (a spectrum with 13 km s^{-1} kinematical resolution is displayed in Fig. 1 of CR96). Assuming a minimum excitation temperature of 100 K, the mass of this component is 4×10^{-4} $M_\odot$, and the momentum carried away is about 0.2 $M_\odot$ km s^{-1}, after correcting for velocity projection effects.

High signal-to-noise ratio $J = 2 \rightarrow 1$ data show that the velocity distribution between the molecular jet and the high-velocity wings is continuous (see e.g., the spectrum obtained near knot S in Fig. 4a). This supports the idea that the high-velocity wings consist of material entrained by/with the jet. *Infrared Space Observatory* (*ISO*) observations of molecular outflows have detected the emission of rotational lines of CO, H$_2$O, and H$_2$ at temperatures between 500 and 1200 K (Nisini et al. 2000; Lefloch et al. 2003). In the case of L1448mm and HH 2, this hot gas emission appears to arise from extreme high-velocity clumps of $2''$ size along the molecular jet. As a conclusion, the hot CO high-velocity emission detected in HH 111 probably traces gas that has been accelerated by internal shocks along the jet.

4.2. *The Physical Conditions*

The single-dish data allow us to determine the physical conditions in the outflowing gas. The CO $J = 2 \rightarrow 1$ and $J = 1 \rightarrow 0$ line intensity both peak at $+9.7$ km s^{-1} (Fig. 2). The gas at this velocity extends along the optical jet. The emission maxima are at positions $-10''$ to $-20''$ away from the exciting source of the HH 111 system; it appears as bright as the main core in the lines of CO and ^{13}CO. In the C^{18}O $J = 1 \rightarrow 0$ line, a secondary component at $+9$ km s^{-1} is detected from $-30''$ to $+60''$ from the
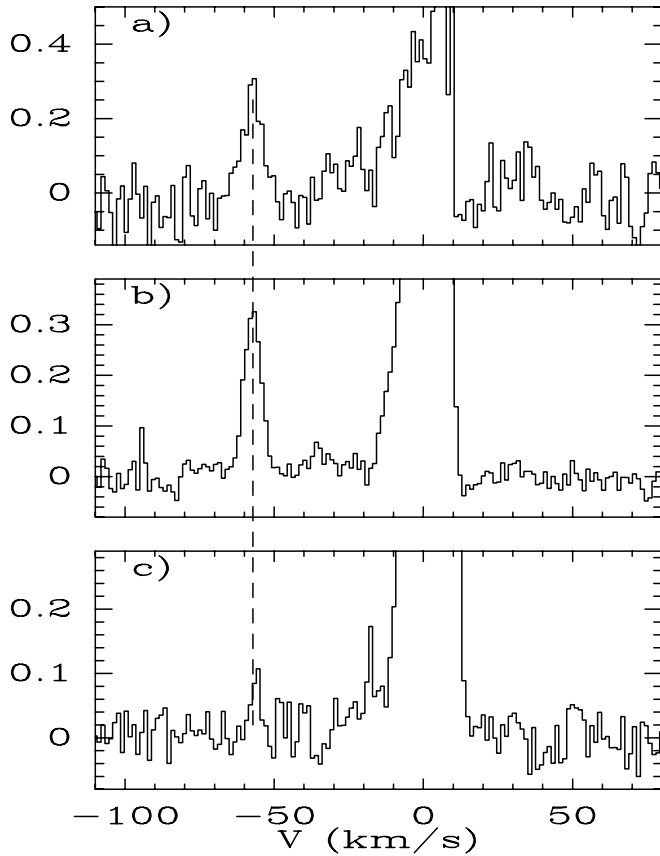
FIG. 4.—High-velocity CO outflow emission detected with the IRAM 30 m telescope beyond the cavity (*a*) at $96''$ from the source, (*b*) near optical knots P–S and (*c*) toward the cavity, within $70''$ from the source.

exciting source along the outflow. A weak counterpart is detected at 7.7 km s^{-1}, about $50''$ from the source, which coincides with the red outflow wing. The parameters of the secondary component were obtained from a Gaussian fit to the C^{18}O lines, which yields a line width of 0.55 km s^{-1}, a brightness temperature of 1.4 K, and an emission peak at +9.2 km s^{-1}. This implies a column density of $\approx 2.5 \times 10^{21}$ cm^{-2}, provided the kinetic temperature is similar to that of the main core, as discussed above. We have estimated the density in the outflow wings from studying the secondary component in the CS lines. After removing the contribution of the main outflow component to the spectra, we have determined from a Gaussian fit main-beam peak temperatures of 1.4 and 0.75 K for the $J = 2 \rightarrow 1$ and $J = 3 \rightarrow 2$ lines from a Gaussian fit, respectively. At a temperature of $20-25$ K, this implies a gas density $n(\mathrm{H_2}) = 7 \times 10^4$ cm^{-3}, and a CS column density $N(\mathrm{CS}) = 7 \times 10^{12}$ cm^{-2}.

4.3. *The PdBI Observations*

We present in Figure 5 the velocity channel maps of the CO $J = 1 \rightarrow 0$ emission between 0 and +13 km s^{-1}, obtained at the PdBI. The maps result from a mosaic of five overlapping fields covering $120'' \times 40''$. Zero-spacing data from the IRAM 30 m telescope has been merged with the PdBI data. The HPBW is $2.5'' \times 3.5''$ and is indicated in the bottom right panel. These observations have a better angular resolution (approximately a factor of 2), sensitivity, and *uv* coverage than the map of Nagar et al. (1997). We have superposed in white the emission of the optical jet, as observed with *HST* in Hα (RHH97). The data confirm the presence of a hollow tubular structure with an outer

diameter of $30''$ (2.1×10^{17} cm), as previously proposed by CR96 and Nagar et al. (1997). Within $30''$ to the source, the geometry of the cavity is well fitted by a parabolic law. However, further away from the source, the gas distribution is better described by a hollow conical cylinder (Fig. 6).

The front and rear sides of the cavity are detected between +2 and +8 km s^{-1} and +8.5 and +12 km, respectively, hence at velocities much lower than the CO outflow (-60 km s^{-1}; CR96). Line widths in the blueshifted gas are rather large, with $\Delta v \approx 4$ km s^{-1} at half power. The walls of the cavity are seen particularly prominent at around +6 km s^{-1}; they present a wider separation, as the distance from the source and the velocity increase (see Fig. 6). *HST* observations in the optical [S II] line indicate that the internal bow shock wings of the jet have a typical diameter of $5''$ (see Figs. 7–11 in RHH97) so that they fill only partly the molecular gas cavity. The walls extend as far as $60''$ away from the source (4.1×10^{17} cm), beyond the HH jet. At $-70''$, we measure an inner separation of $8''$ between the walls, which corresponds to an opening angle of $5°$. This separation is also the distance between the wings of the bow shock observed in the jet at this position. Emission at extreme velocities of +2.5 and +10.5 km s^{-1} is detected along the jet main axis, which provides a measurement of the expansion of the cavity around the jet. We derive an average radial expansion velocity of ≈ 4 km s^{-1}. This implies a kinematical age of 8700 yr for the outermost gas layers in the expanding cavity, at $15''$ away from the optical jet axis. This is similar to the kinematical age of the optical jet (CR96).

The velocity distribution on the rear side of the cavity provides strong constraints on its geometry. The emission of the rear wall of the cavity is detected at about 9 km s^{-1} west of the source, where the outflow propagates at *blueshifted* velocities [see panel at offset position $(-20, 0)$ in Fig. 2]. The emission of the rear wall is characterized by relatively narrow line widths (1–2 km s^{-1}) and low-velocity motions with respect to the cloud gas, much smaller than those detected on the front side. This implies that the rear side lies close to the plane of the sky, in agreement with the $\sim 10°$ angle of the optical jet to the plane of the sky derived by Reipurth et al. (1992) and the above opening angle of $5°$. The velocity distribution undergoes a *positive gradient* with increasing distance to the source, up to offset $+50''$ along the jet. As the jet is blueshifted, this positive gradient is naturally explained if the tangential velocity is much larger than the component normal to the wall.

We present in Figure 7 the CO intensity distribution as a function of velocity in cuts made parallel to the jet direction. Emission from the front cavity walls is detected from $-11''$ to $+11''$ from the jet axis. The location of the front and rear cavity walls is marked with thick white lines, in the cut made along the jet axis (offset $-0.4''$). The velocity shift between the front and the rear wall increases strongly with distance x to the source, which implies that the tangential velocity also increases. The velocity field of the front and rear walls is well described by a linear law $v \propto x$; the corresponding fits are displayed in Fig. 7.

The maximum velocity (≈ 1 km s^{-1}) is observed ahead of the optical jet. A small gas knot is detected at the tip of the jet between offsets $-45''$ (bow shock L) and $-60''$ (knot O) in the panel at +1.4 km s^{-1} (see Fig. 5). A counterpart to this knot is detected in the redshifted gas, at +9.5 km s^{-1}. Emission at a lower velocity (+2.4 km s^{-1}) is detected upstream of the knot and off the jet axis (Fig. 5). The whole wall appears to be accelerated along the optical jet up to this knot, as can be seen on the cuts at $-11''$ and $+2.4''$ in Fig. 7. About $5''$ downstream of knot O, the wings of bow shock P are detected (Fig. 8 in RHH97). Those wings are remarkably extended, $10''$, comparable to the width of the inner
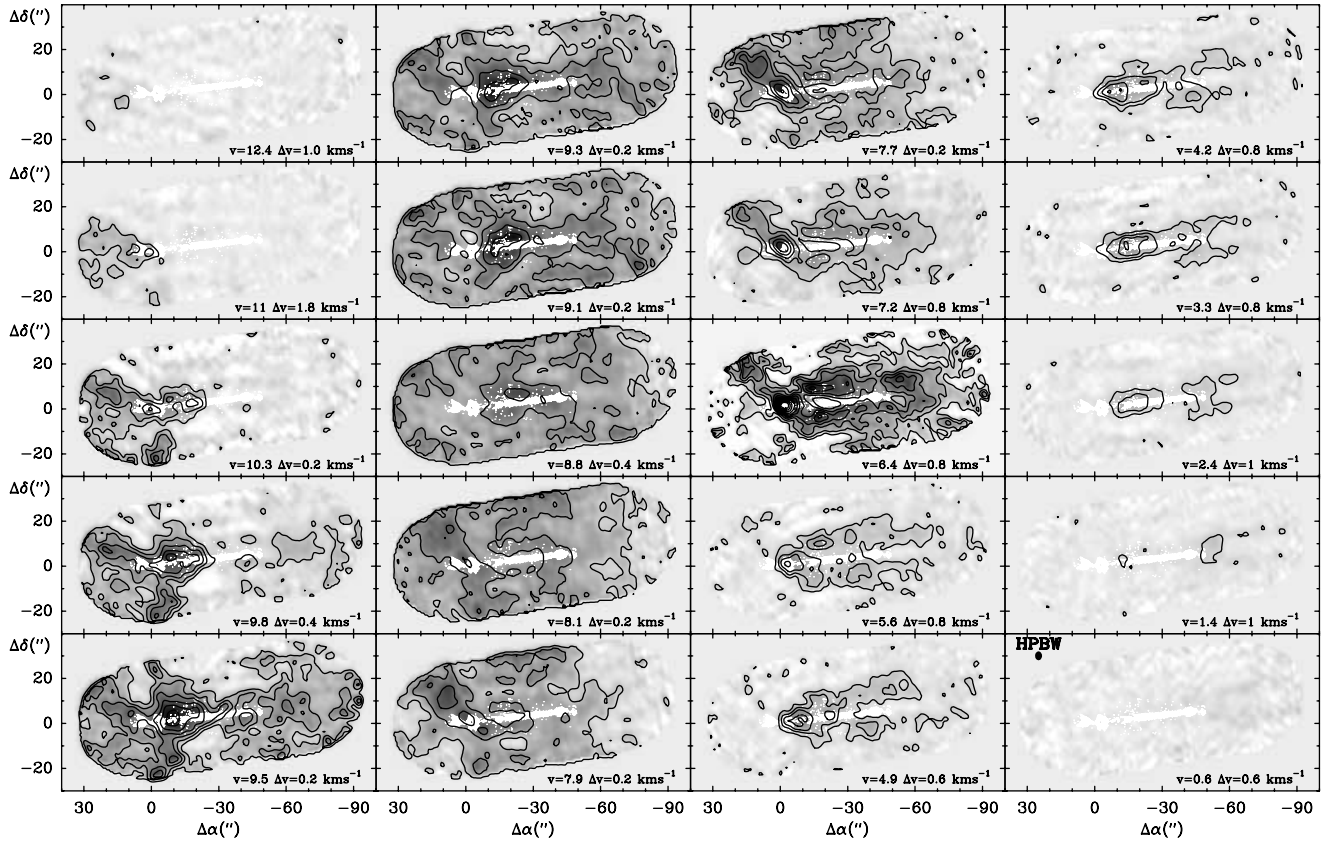
FIG. 5.— Interferometric map of the CO $J = 1 \rightarrow 0$ emission in HH 111. The optical HH jet, as observed with *HST*, is drawn in white. The synthetic beam ($2.5'' \times 3.5''$ HPBW) is indicated in the bottom right panel. First contour and contour interval in the various panels are 0.6 K in the first column; 0.6 and 0.9 K, respectively, in the second column; 0.6 K for the panels at 7.7 and 7.2 km s^{-1}, 0.6 and 1.0 for the panel at 6.4 km s^{-1}, and 0.4 K for the panels at 5.6 and 4.9 km s^{-1} in the third column; and 0.4 K in the fourth column.
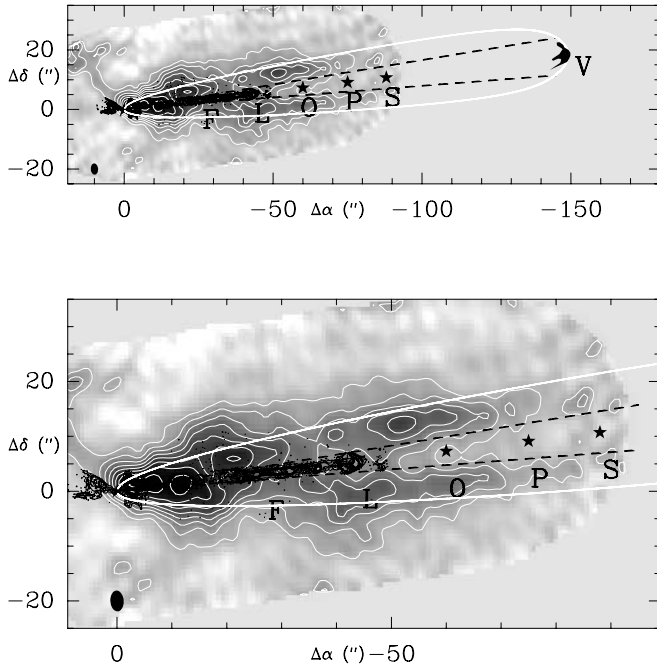

FIG. 6.— *Top*: Map of the CO $J = 1 \rightarrow 0$ emission integrated between +0.25 and +7.3 km s^{-1}. The position of optical knots along the jet is marked with squares. The white line fits the cavity of gas swept up in the propagation of bow shock V. Two dashed lines mark the opening of the cavity inner walls. The synthesized beam is drawn in the bottom left corner. Contours range from 0.2 to 1.1 with steps of 0.1×7.1 Jy beam km s^{-1}. *Bottom*: Magnified view of the CO cavity.

cavity "hole." The molecular gas has probably been accelerated in the wings of bow shock P.

Near the source, the gas undergoes a strong acceleration, which terminates at the location of optical knot F, at 27″ from the source (Figs. 4 and 5; RHH97). A symmetrical feature displaying a strong gas acceleration is also detected, which extends up to +15″ east of the source. Both components are marked by a white dashed line in Figure 7.

We suggest that both features are tracing a recent ejection from the protostellar source, associated with knots E and F. This gas component extends from −6″ up to +5″ from the jet main axis (Fig. 7); hence, the ejection takes place inside the large-scale cavity reported above. Indeed, based on Space Telescope Imaging Spectrograph (STIS) spectroscopic data of the jet obtained with *HST*, Raga et al. (2002) showed good evidence that optical knot F traces an internal working surface resulting from time variability in the ejection velocity, on a scale of 250 yr.

The velocity field appears much more complex (see panel at −0.4″ in Fig. 7). It can be fitted by a linear law between the source and offset $\Delta\alpha = -20''$. One can note that the linewidth gets broader with decreasing distance to knot F, in panels at −3.2″, +2.4″, and along the jet. Between −25″ and −40″ the CO emission covers a broader range of velocities. Such broadening could trace gas accelerated by knots E and F or in previous events like bow shock L.

5. THE CO BULLETS

Beyond the optical bow shock V, CR96 discovered three CO bullets (hereafter referred to as Bullet 1, 2, and 3, in order of increasing distance from the source) with separations of $\simeq 55''$.
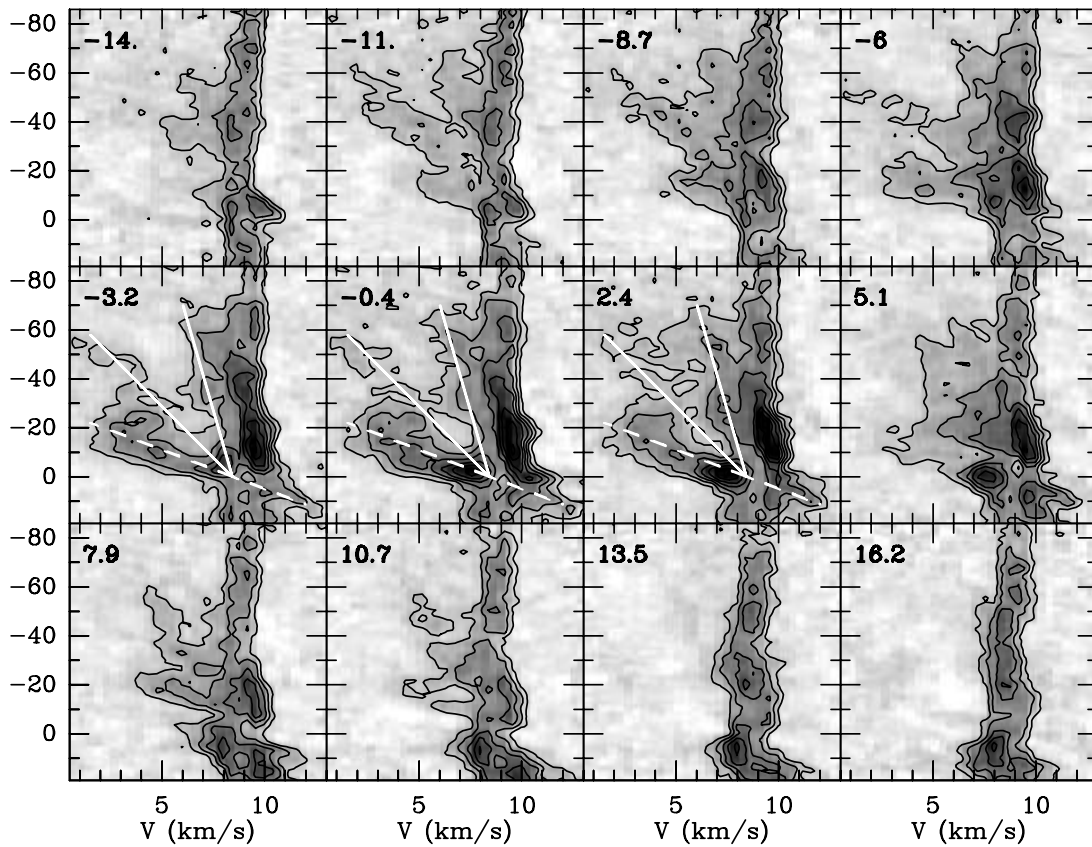
FIG. 7.—Velocity-position diagram of the CO $J = 1 \rightarrow 0$ emission along cuts parallel to the HH jet. Positive (negative) cuts are made north (south) of the jet axis. Distance to the jet (in arcseconds) is indicated in the top left corner of each panel. First contour and contour interval is 0.5 Jy beam^{-1} (3.7 K). In the cut at $-0.4''$ from the jet axis, we have indicated with solid white lines the front and rear cavity walls. White dashed lines mark the direction of the secondary CO component.

No optical emission is associated with these bullets. However, they are perfectly aligned along the direction defined by the optical jet. Whereas the optical knots P and V are tracing shocked material, the molecular bullets B1–B3 have no heating source. Based on the association of optical knots with some high-velocity bullets, CR96 proposed that the latter bullets were tracing past shock episodes of HH 111.

5.1. *The PdBI Observations*

High angular resolution maps have been obtained with the PdBI interferometer in the CO $J = 2 \rightarrow 1$ line (Fig. 8). The emission properties of all three bullets are very similar. The molecular emission from the bullets was marginally resolved by

the IRAM 30 m telescope; it allowed us to estimate a size of $8''–10''$. The much better angular resolution of the PdBI observations allows us to resolve the emission. Each bullet is elongated in the north-south direction; the large-scale distribution is well described by an ellipse with typical size (beam deconvolved) of $3'' \times 7''$ ($2.0 \times 4.8 \times 10^{16}$ cm). We note that the transverse size of the bullets ($\simeq 10''$) matches reasonably well the inner diameter of the cavity around the jet.

Each bullet presents a complex kinematical structure down to arcsecond scale (Fig. 9). The line profiles are characterized by a broad plateau, spanning $10–15$ km s^{-1}, and a line core of 5 km s^{-1} HPFW. To study the gas kinematics in the bullets, we have considered separately the spatial distributions of the blue and red
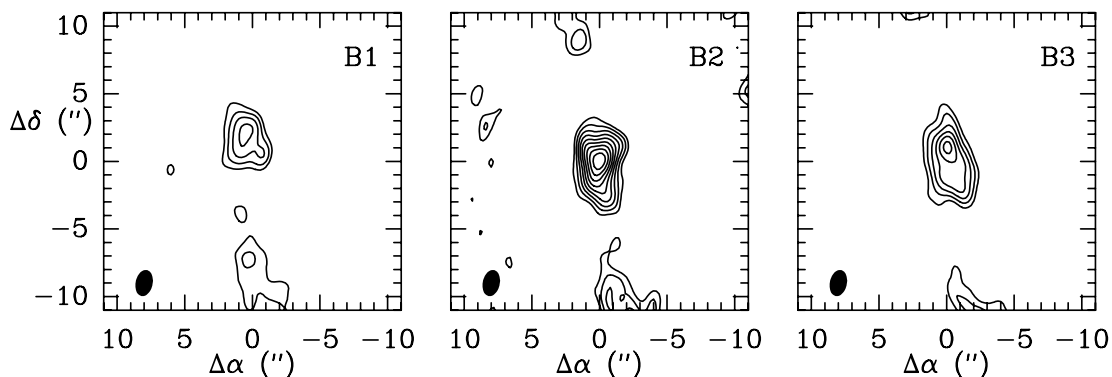

FIG. 8.—Interferometric maps of the velocity-integrated flux in the bullets B1–B3 in the CO $J = 2 \rightarrow 1$ transition. The first contour and interval are 0.10 and 0.04 Jy beam^{-1}, respectively.
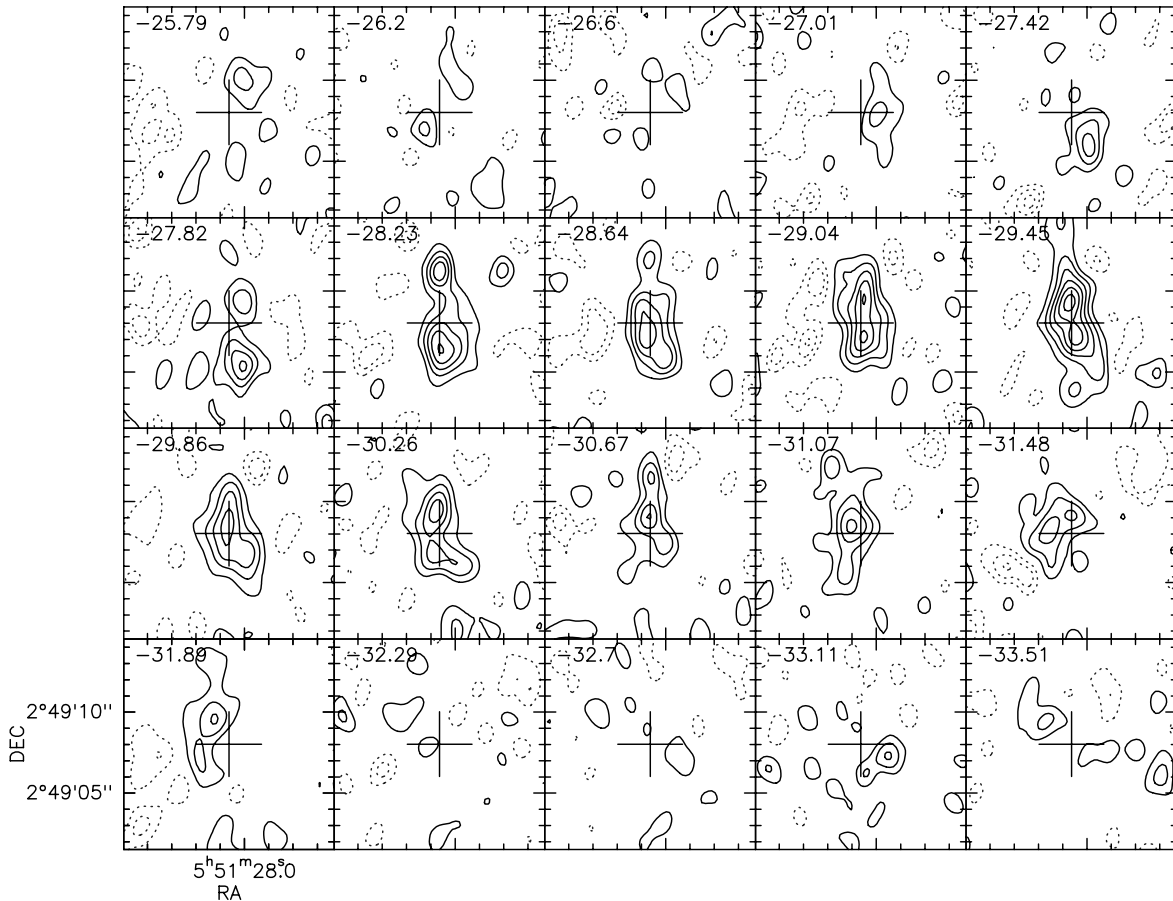
Fig. 9.—Map of the $J = 2 \rightarrow 1$ emission in B3, integrated in velocity intervals of 0.4 km s^{-1}. Contour interval is 0.2 Jy beam^{-1} (1.87 K).

wings (Fig. 10). In all three bullets, the blueshifted component appears to lie $\approx 1''$ (1 beam size) upstream of the redshifted component. It suggests a sideways expansion of the bullets, which now propagate in a low-density medium, and are oriented at only a small angle out of the plane of the sky.

5.2. *The Physical Conditions*

Hatchell et al. (1999) observed at the James Clerk Maxwell Telescope (JCMT) the CO $J = 4 \rightarrow 3$ and $J = 3 \rightarrow 2$ emission near optical knot P, bow shock V, and bullet B3. Under the hypothesis that the levels are populated at local thermodynamic equilibrium (LTE) and the lines are optically thin, they estimated a kinetic temperature of $\simeq 100$ K in the high-velocity ejecta. It is in bullet B3 that these authors derive the highest temperature, around 270 K. This is rather unexpected, as B3 is the most distant bullet from the source. We note that the transitions observed by the authors are not well suited to trace such high-temperature gas. Higher J transitions of CO are more sensitive probes of the kinetic temperature.

We have carried out an LVG analysis of the CO line fluxes measured toward B3, based on the data of CR96 and Hatchell et al. (1999). We have first corrected for the beam dilution, especially critical for the $J = 1 \rightarrow 0$ transition, adopting a bullet size of $10''$, in agreement with CR96 and our PdBI observations (see below). We adopted an average line width $\Delta v = 5.5$ km s^{-1}, from the 30 m and PdBI observations. We conclude that it is not possible to reproduce simultaneously all four transitions. The observed $J = 4 \rightarrow 3$ flux exceeds by a large factor (about 4) the intensity predicted by the model. It is in fact the high flux measured in this transition that is responsible for the high temperature derived by Hatchell et al. (1999). However, there is no

evidence for internal shocks, which would heat the bullet material to such high temperatures. As discussed below, the cooling timescale of this gas is very short, so its temperature should decrease much below the 100–150 K measured in the optical knots P–V. We conclude that most likely the $J = 4 \rightarrow 3$ line intensity was highly overestimated. As pointed out by Hatchell et al. (1999), the calibration of the 460 GHz receiver was highly uncertain at the time of the $J = 4 \rightarrow 3$ observations.

If we repeat the analysis considering only the first three CO transitions and taking into account the uncertainty in the measured flux (about 10%), a good agreement is obtained for a CO column density $N(CO) = 1.2 \times 10^{16}$ cm^{-2}. The best agreement is then obtained for temperatures in the range 35–45 K and H$_2$ densities in the range $(5-8) \times 10^3$ cm^{-3} (see below).

Neufeld et al. (1993, 1995) have studied the radiative cooling of warm molecular gas $T \geq 100$ K in various astrophysical environments. Applying their work to the case of the HH 111 bullets, we estimate a typical cooling time of 600 yr if the temperature of the bullets is as high as 100 K. This is approximately the typical flight time between two subsequent molecular bullets (500 yr). The distance from bullet V, the last one for which we observe evidence of a shock, to bullet B3 is $120''$, which needs about 1500 yr to be crossed, almost 3 times the CO cooling time.

We conclude that although the temperature of the bullets inside the molecular cloud is about 100–150 K, the molecular bullets B1–B3 are most likely made of colder gas, at a temperature of typically 35–45 K. Under such physical conditions [$n(H_2) = 8000$ cm^{-3} and $N(CO) = 1.2 \times 10^{16}$ cm^{-2}], the $J = 2 \rightarrow 1$ transition is optically thin, $\tau \simeq 0.3$, and has an excitation temperature $T_{ex} \simeq 20$ K. This is slightly larger than the value derived
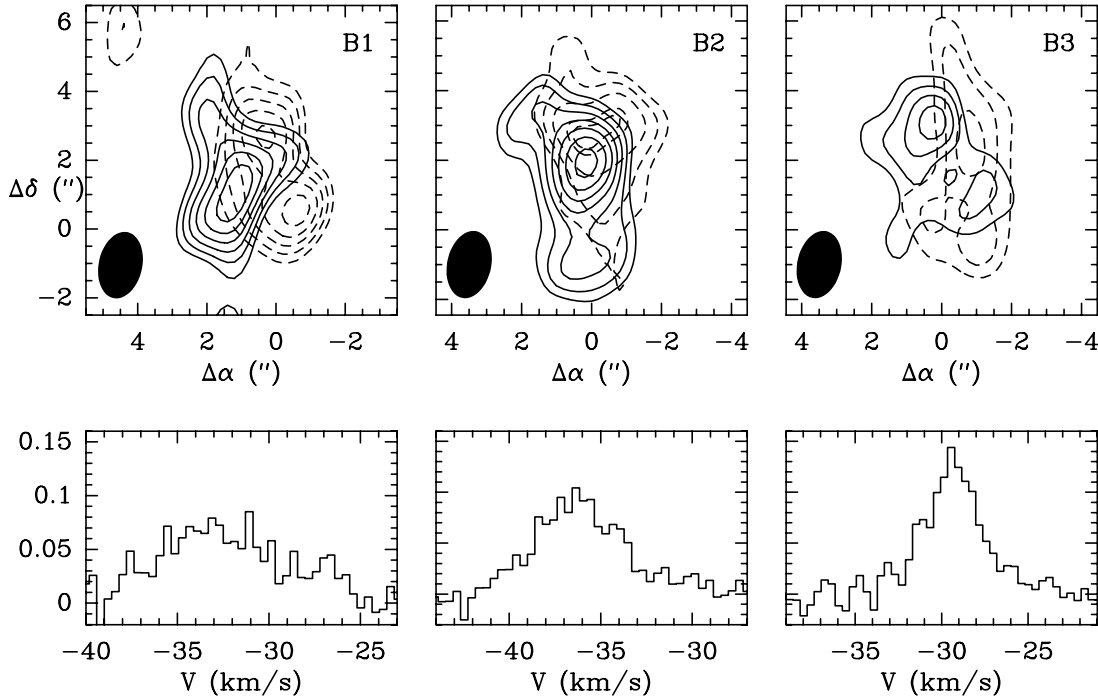
Fig. 10.—*Bottom*: Average spectrum of the bullets, in the region of intensity larger than 50% the brightness peak. *Top*: Blueshifted (redshifted) emission is shown by solid (dashed) contours. First contour and contour interval are 0.10 and 0.04 Jy beam^{-1}, respectively.

by CR96 (15 K), although the other physical parameters (mass, mass transport rate and momentum) are essentially unchanged.

From the above timescale, we estimate a time-averaged mass transport of $4 \times 10^{-7}\, M_\odot$ yr^{-1}, whereas Hartigan et al. (1994) derive a mass-loss rate of $1.8 \times 10^{-7}\, M_\odot$ yr^{-1}. The similar mass transport rates support the view that the CO bullets are not made of ambient material that has been accelerated to these very high velocities, but are mostly composed of material ejected from the central engine. The momentum carried away by each bullet amounts to $1.0 \times 10^{-4} M_\odot$ km s^{-1} yr^{-1}.

Raga et al. (1990, 2002) proposed that optical knots form from time variable gas ejections in the jet. Such mechanism leads to the formation of "minibows" along the jet. In this framework, the high-velocity CO bullets would trace the previously shocked molecular counterpart of the optical knots. It naturally explains the similar properties observed between the jet and the high-velocity bullets (size, kinematics, and momentum). The weak high-velocity component detected between B1 and B2 (see Fig. 6 in CR96) traces the molecular "intershock" gas ejected from the central source, between two "eruptions."

6. GAS ENTRAINMENT MECHANISM

6.1. *The Cavity*

The kinematics of the outflowing gas is complex as it bears the signature of several ejection episodes in the optical jet, associated with bow shocks at knots F and L (RHH97; Raga et al. 2002). We also find a strong correlation between the low- and high-velocity outflow wings and the jet. It is therefore unlikely that a single fit of any outflow model is able to reproduce the kinematics of the gas observed along the whole flow length. As the ejecta are located inside the cavity, close to the source (within $\approx 30''$), we have decided to concentrate on the global properties of the cavity, at greater distance from the source. Our interferometric data have revealed a large cylindrical cavity in which the gas is accelerated following a "Hubble law" $v \propto x$ distance along the jet axis.

The formation of such large cavities is easily accounted for by the sweeping up of ambient material as a bow shock propagates into the parental cloud (RC93). In what follows, we show that such gas entrainment models can indeed account for the molecular outflow emission in HH 111. We first determine the parameters of the "best" model that fits the HH 111 molecular gas distribution.

As shown by RC93, the global shape of the cavity swept up by an internal bow shock depends on two parameters: the density stratification of the ambient medium and the ratio between the distance of the working surface to the source d and the standoff distance between the working surface and the bow shock apex r_s.

For a jet propagating into a medium of density $\rho \propto x^\beta$, where x measures the distance from the powering source along the jet axis, the following relation holds between the jet cylindrical radius r_c and x, $r_c \propto x^{-\beta/2}$. As discussed above and in § 4.3, the shape of the cavity *near* the source is suggestive of $\beta = -1$.

The standoff distance r_s between the ejection point in the working surface and the bow shock apex is related to the jet radius via

$$r_s = r_j \left(\frac{\pi \rho_j}{\Omega \rho_a} \right)^{1/2} \left(\frac{v_0}{v_j} \right), \qquad (1)$$

where Ω is the solid angle over which mass is ejected ($\Omega \approx 2\pi\sqrt{2}$), and v_0 and v_j are the ejection and jet velocities, respectively (see eq. [4] in RC93).

In the case of strong working surfaces such as those observed in HH 111, the ratio between the jet and the ambient density ρ_j/ρ_a is $\simeq 100$ (Raga & Binette 1991) and $v_0 \simeq v_j$ in the adiabatic case. Hence, $r_s/r_j \simeq 6(v_0/v_j) \leq 6$ and $r_s \leq 9''$, with a typical jet radius of $1.5''$ (RHH97).

A simple determination comes from the shape of the cavity computed in the case $\beta = -1$. The cylindrical radius is typically twice the standoff distance (see, for example, the top panel of Fig. 3); it is not very sensitive to the actual value of β nor to the

distance of the bow shock to the source. At zeroth order the diameter of the cavity determined in the outer part is $\approx 18'' = 4r_s$, hence $r_s \approx 4.5''$. This simple determination is consistent with the upper limit obtained previously. It is also consistent with numerical simulations, which yield $r_s/r_j \sim 3$.

Since bow shock V lies at $148''$ from the source (RHH97), one has $d/r_s = 32$. We display in Figure 6 the shape of the cavity swept up by a bow shock as predicted for this set of parameters. This model fits nicely the walls of the cavity and the curvature of bow shock V. The agreement is very satisfying at $\Delta \alpha \leq -50''$. We have fitted the inner walls of the cavity by straight lines (drawn in dashed dark contours in Fig. 6); the optical jet emission appears to fill exactly the cavity walls up to $\Delta \alpha = -50''$. Extrapolating the fit up to bow shock V, we find that the separation of the walls at that position is $\sim 10''$. It matches well the size of the bow shock in the Hα optical line (see top panel of Fig. 6), as expected for freely expanding shocked material.

For values of β of -1, the model predicts that the velocity versus position along the axis is almost exactly linear over the whole flow length, except close to the source. This is again consistent with the position-velocity diagram derived from our interferometric maps (see Fig. 7).

The situation is more complex closer to the source; molecular gas emission is still detected beyond the fit, so the agreement between the fit and the actual shape of the cavity is not very good. Several factors may contribute to this. In particular, several ejections have taken place recently, which are now observed as knots E to L. Since this part of the cavity has experienced the crossing of two more bow shocks (P and L), the walls have been transferred additional momentum. This could contribute to our detection of entrained gas at further distances from the jet axis.

These results differ somewhat from the previous conclusions of Nagar et al. (1997). Based on their interferometric map of the CO $J = 1 \rightarrow 0$ line emission, these authors interpreted the velocity field and the spatial distribution of the molecular gas as evidence for an outflow entrained by a wide-angle radial wind, as modeled by Shu et al. (1991, 1995). The modeling of the position-velocity diagram of the emission along the jet is indeed in good agreement with the predictions of radial-wind-driven outflows (Li & Shu 1996). As pointed out by Cabrit et al. (1997), a simple fit to the position-velocity distribution of the outflowing gas does not allow one to discriminate between jet-driven and wide-angle wind models, when the inclination with respect to the plane of the sky is low.

We note that the physical conditions close to the source (less than $15''$) play an important role in constraining the parameters of the wide-angle wind fitted by Nagar et al. (1997). As can be seen in their Figure 5, it appears that at larger distances the radius of the cavity is constant rather than parabolic-like, as claimed by the authors, and the match between the observed velocity profile and the fit is less satisfying.

In our opinion, the strong ejection activity near the source prevents conclusions about the role of a wide-angle wind in driving molecular gas, as these ejecta are very efficient at transferring momentum to the ambient material. Interferometric observations at a higher angular resolution than the data presented here are required to investigate the relation the optical shocked knots hold to the molecular gas and how the dynamics of the cavity is affected.

However, the formation of the large-scale cavity observed up to bow shock P is well explained in the frame of the model of RC93. The jet entrains ambient molecular material swept up in the propagation of bow shocks, which disturb the ambient gas at large distances from the jet axis. Our observations indicate that bow shock V played a major role in shaping the global cavity.

6.2. *The Hot Gas Component*

Our observations of the CO 7–6 emission bring evidence for hot outflowing gas in the cavity that is missed by observations of the low-J transitions due to the extremely low opacity of the latter. This is evidenced by the maximum radial velocity detected in the outflow wings in the $J = 7 \rightarrow 6$ and $J = 2 \rightarrow 1$ transitions (30 and 10 km s^{-1}, respectively). It is therefore necessary to take into account the thermal structure of the outflow to discriminate between the various gas acceleration mechanisms that have been proposed.

The hot gas component probably occupies a much smaller region than the low-velocity cold gas, with a typical size of the emitting region of a few arcseconds. The emission likely arises from shocked gas in the jet, a conclusion supported by the high velocities and temperature measured in this gas. High signal-to-noise ratio spectra obtained further downstream in the jet show a continuous velocity distribution between the molecular jet and the high-velocity wings, and support a close association between both phenomena. [C I] observations do not show any evidence of CO dissociation close to the source; hence, the gas is probably accelerated in C-type, rather than J-type shocks, along the jet.

Averaging the CO $J = 2 \rightarrow 1$ signal over the cavity reveals a faint molecular jet signature at 60 km s^{-1}, consistent with the velocity of the molecular features (bullets) detected further downstream (Fig. 4). The presence of such a hot component shows that there is no clear velocity separation between the outflowing gas and the jet itself (see Fig. 4; see also bottom panel of Fig. 1 in CR96). Interferometric observations with the SMA in the CO $J = 6 \rightarrow 5$ transition would allow one to determine the location of the emission. Observations of the high-J CO lines with the *Herschel Space Observatory* would allow clarification of the physical conditions in the outflowing gas.

7. CONCLUSIONS

We have presented single-dish and interferometric line observations of the HH 111 outflow and its driving source. The physical conditions of the protostellar core were determined from the emission of the millimeter lines of CO and its isotopomers, the millimeter lines of CS, all of them observed with the IRAM 30 m telescope, and the CO $J = 7 \rightarrow 6$ line observed with the CSO. The molecular gas emission reveals a small condensation of cold ($T = 20$–25 K) and dense gas [$n(H_2) = 3 \times 10^5$ cm^{-3}].

The low-velocity outflowing gas has been mapped with the IRAM Plateau de Bure interferometer. It is distributed in a hollow cylinder that surrounds the optical jet. The formation of this cavity and its kinematics are well accounted for in the frame of the model of RC93. The jet entrains ambient molecular material swept up in the propagation of bow shocks, which disturb the ambient gas at large distances from the jet axis. Our observations indicate that bow shock V played a major role in shaping the global cavity. The gas velocity is found to vary almost linearly with distance to the source over the whole flow length, except close to the source. The cavity has been expanding with a mean velocity of 4 km s^{-1} on a timescale of 8700 yr, similar to the dynamical age of the optical jet. The separation of the inner walls reaches $8''$–$10''$ near knots P and S, which corresponds to the transverse size of the wings in these bow shocks.

The more recent ejections detected close to the source are still efficient at transferring momentum to the ambient material. Regions of strong gas acceleration are detected along the jet, which are correlated with the optical bow shocks at knots F and L.

Observations of the high-excitation line CO $J = 7 \rightarrow 6$ reveal high-velocity outflowing gas ($v = 150$ km s^{-1} after deprojection)

near the central source. This high-velocity component is hot ($T = 300–1000$ K) and fills only a small fraction of the beam. We propose that this emission arises from shocked gas in the optical jet.

Emission of the molecular bullets B1–B3 was mapped with the IRAM PdBI in the CO $J = 2 \rightarrow 1$ transition. The emission is distributed in structures of $3'' \times 7''$ flattened perpendicularly to the jet main axis. Their kinematics are complex, but an overall sideways expanding motion is detected inside all of them. Their physical properties have been reassessed; we find a low temper-

ature for the bullets ($\sim$30 K), in agreement with the cooling timescale for shocked gas initially heated at temperatures of 100 K or greater and cooling down while flying freely. Their density lies now in the range $(0.5–1.0) \times 10^4$ cm^{-3}. These molecular bullets probably form in the shocks resulting from time-variable ejections in the powering source, in the manner proposed by Raga et al. (2002) to account for the presence of mini bow shocks and knots in the optical jet. In such a scenario, the weak high-velocity molecular jet detected between the molecular bullets represents intershocked gas ejected from the central source.

REFERENCES

Cabrit, S., Raga, A., & Gueth, F. 1997, in IAU Symp. 182, Herbig-Haro Flows and the Birth of Low Mass Stars, ed. B. Reipurth & C. Bertout (Dordrecht: Kluwer), 163
Cernicharo, J., Neri, R., & Reipurth, B. 1997, in IAU Symp. 182, Herbig-Haro Flows and the Birth of Low Mass Stars, ed. B. Reipurth & C. Bertout (Dordrecht: Kluwer), 141
Cernicharo, J., & Reipurth, B. 1996, ApJ, 460, L57 (CR96)
Coppin, K. E. K., Davis, C. J., & Micono, M. 1998, MNRAS, 301, L10
Davis, C. J., Mundt, R., & Eislöffel, J. 1994, ApJ, 437, L55
Dent, W. R. F., Matthews, H. E., & Ward-Thompson, D. 1998, MNRAS, 301, 1049
Flower, D. 2001, J. Phys., B., 34, 2731
Gredel, R., & Reipurth, B. 1993, ApJ, 407, L29
———. 1994, A&A, 289, L19
Hartigan, P., Morse, J. A., & Raymond, J. 1994, ApJ, 436, 125
Hatchell, J., Fuller, G. A., & Ladd, E. F. 1999, A&A, 346, 278
Lee, C.-F., Mundy, L. G., Reipurth, B., Ostriker, E. C., & Stone, J. M. 2000, ApJ, 542, 925
Lefloch, B., et al. 2003, ApJ, 590, L41
Li, Z. Y., & Shu, F. H. 1996, ApJ, 468, 261
Morse, J. A., Heathcote, S., Cecil, G., Hartigan, P., & Raymond, J. C. 1993a, ApJ, 410, 764
Morse, J. A., Heathcote, S., Hartigan, P., & Cecil, G. 1993b, AJ, 106, 1139
Nagar, N. M., Vogel, S. N., Stone, J. M., & Ostriker, E. C. 1997, ApJ, 482, L195

Neufeld, D. A., & Kaufman, M. J., 1993, ApJ, 418, 263
Neufeld, D. A., Lepp, S., & Melnick, G. J. 1995, ApJS, 100, 132
Nisini, B., et al. 2000, A&A, 360, 297
Noriega-Crespo, A., Garnavich, P. M., & Raga, A. C. 1993, AJ, 106, 1133
Raga, A. C., & Binette, L. 1991, Rev. Mex. AA, 22, 265
Raga, A. C., Binette, L., Cantó, J., & Calvet, N. 1990, ApJ, 364, 601
Raga, A. C., & Cabrit, S. 1993, A&A, 278, 267 (RC93)
Raga, A. C., et al. 2002, ApJ, 565, L29
Reipurth, B. 1989, Nature, 340, 42
———. 2000, AJ, 120, 3177
Reipurth, B., & Bally, J. 2001, ARA&A, 39, 403
Reipurth, B., Bally, J., & Devine, D. 1997a, AJ, 114, 2708
Reipurth, B., & Cernicharo, J. 1995, Rev. Mex. AA Ser. Conf., 1, 43
Reipurth, B., & Olberg, M. 1991, A&A, 246, 535
Reipurth, B., Raga, A. C., & Heathcote, S. 1992, ApJ, 392, 145
Reipurth, B., et al. 1993, A&A, 273, 221
———. 1997b, AJ, 114, 757 (RHH97)
———. 1999, A&A, 352, L83
———. 2000, AJ, 120, 1449
Rodríguez, L. F., & Reipurth, B. 1994, A&A, 281, 882
Shu, F. H., Najita, J., Ostriker, E. C., & Shang, H. 1995, ApJ, 455, L155
Shu, F. H., Ruden, S. P., Lada, C. J., & Lizano, S. 1991, ApJ, 370, L31
Stapelfeldt, K., & Scoville, N. Z. 1993, ApJ, 408, 239
Yang, J., et al. 1997, ApJ, 475, 683